Appl Phys B (2011) 105:575–582
DOI 10.1007/s00340-011-4512-5

Applied Physics B
Lasers and Optics

A precise and wide-dynamic-range displacement-measuring homodyne quadrature laser interferometer

T. Požar · P. Gregorčič · J. Možina

Received: 23 October 2010 / Revised version: 1 April 2011 / Published online: 29 April 2011

Abstract We present a fast, displacement-measuring, single-pass, two-detector homodyne quadrature laser interferometer and compare its performance with an arm-compensated, proportional, integral-derivative-controlled Michelson interferometer. Special attention is given to the extension of the dynamic range. The wide dynamic range is achieved by an accurate fringe subdivision based on an enhanced ellipse-specific fitting of the scattered Lissajous curve and by increasing the total displacement using the quadrature-detection technique. The common periodic deviations, i.e., the unequal AC amplitudes, the DC offsets, and the lack of quadrature are determined and reduced by data processing based on an ellipse-specific, least-squares fitting to obtain nanometric accuracy. The performance of the described interferometer is demonstrated through the measurement of high-amplitude and high-frequency laser-induced ultrasound.

1 Introduction

Several measurements of displacement [1, 2] demand a wide dynamic range. This dynamic range is defined as the total displacement (which can be reached at a given resolution) divided by the resolution. Thus, to have a wide dynamic range, the resolution has to be improved and the total displacement extended. The resolution can be improved by a uniform fringe subdivision, while the total displacement can be increased by employing the quadrature detection. When laser interferometry is used for displacement measurements, the limiting resolution is dictated by the photon shot noise [3].

A wide dynamic range is achieved with homodyne quadrature laser interferometers (HQLIs) [4, 5]. HQLIs are a special extension of arm-compensated Michelson interferometers (ACMI) [6] that feature a dynamic range of less than 10^4. The considerably improved dynamic range of HQLIs over ACMIs is obtained by employing the quadrature-detection technique, which extends the total displacement while preserving the resolution. Here, the quadrature detection is achieved using a stable, linearly polarized laser, and adding an additional octadic-wave plate and a polarizing beamsplitter to obtain two orthogonally polarized interference signals in phase quadrature that are detected by two photodiodes. These two signals provide the means to measure the displacements with a sub-nanometer resolution and constant sensitivity over displacements of at least 1 mm. If the index of refraction is further compensated by measuring the temperature, pressure, humidity, and carbon dioxide content using empirical equations [7], displacements of almost 0.1 m can be measured with an accuracy of 1 nm [8].

This paper presents the simplest modification of the ACMI—the single-pass, two-detector homodyne quadrature laser interferometer. It describes the operation of an ideal and practical realization of the HQLI. The common nonlinearities that reduce the accuracy by introducing the fringe-periodic errors in the measured displacement are discussed and effectively corrected using the technique first introduced by Heydemann [9], but employing the recently developed fitting method given by Harker et al. [10]. This novel data processing based on a special, ellipse-specific, least-squares-fitting algorithm features a robust and stable fringe subdivision with nanometric resolution. Since our HQLI uses fast, 200-MHz photodiodes, it is applicable for the measurements of motion induced by high-intensity laser

T. Požar (✉) · P. Gregorčič · J. Možina
Faculty of Mechanical Engineering, University of Ljubljana,
Aškerčeva 6, 1000 Ljubljana, Slovenia
e-mail: tomaz.pozar@fs.uni-lj.si

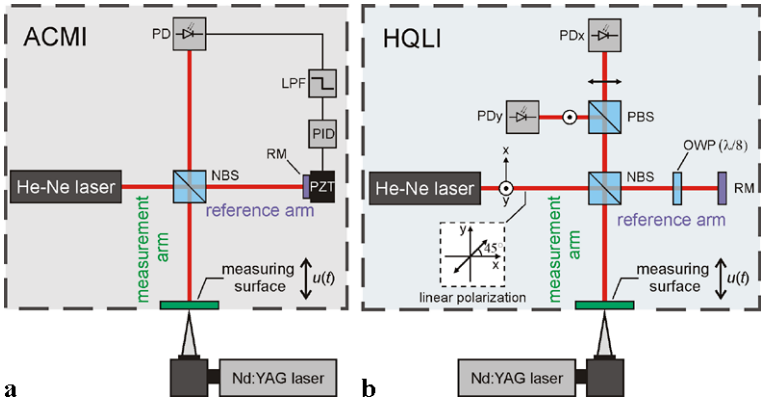

Fig. 1 (**a**) Schematic top view of the ACMI. The interferometer is locked to the most sensitive point using a 1-kHz low-pass filter (LPF), the proportional integral-derivative controller (PID), and the reference mirror (RM) attached to the piezoelectric transducer (PZT). The motion of the measuring surface is detected by a single photodiode (PD). (**b**) The HQLI consists of: the stabilized ($\lambda = 632.8$ nm; amplitude stability over 1 min <0.2% and amplitude noise (0–10 MHz) <0.2%) and linearly polarized He–Ne laser beam at 45°, the measuring surface, the RM, the octadic-wave plate (OWP), the non-polarizing beamsplitter (NBS), the polarizing beamsplitter (PBS), the two photodiodes measuring the x-polarized (PDx), and the y-polarized (PDy) light. The time-dependent normal displacement $u(t)$ is encoded in the optical phase $p(t)$. The high-amplitude ultrasound is induced by a pulsed Nd:YAG laser

pulses. We give a concise comparison between the common ACMI and the HQLI. Besides the theoretical comparison, their performance is examined experimentally by monitoring the high-amplitude and high-frequency laser-induced ultrasound on an aluminum plate.

2 Ideal homodyne quadrature laser interferometer

We will first shortly review the limitations of the Michelson interferometer (MI), which is schematically illustrated in Fig. 1a. In the case of an ideal MI, the time-dependent output voltage signal $x(t)$ taken from the photodiode PD varies as a harmonic function (see Fig. 2b) if the measuring surface moves uniformly along the path of the laser beam. Assuming that the photodiode has a linear response, the ideal interference signal with perfect visibility has the following form:

$$x(t) = \frac{V_0}{2}\big(1 + \sin p(t)\big) = \frac{V_0}{2}\left(1 + \sin\left(\frac{4\pi u(t)}{\lambda}\right)\right), \quad (1)$$

where p is the optical phase difference between the beams from separate arms from which the displacement $u = \lambda/(4\pi)p$ is inferred. V_0 is the output photodiode voltage if the whole laser light of wavelength λ was collected by a single photodiode.

A more general form of the interference signal can be written as

$$x = x_0 + A_x \sin p. \quad (2)$$

Here, x_0 stands for the DC offset and A_x for the AC amplitude. Ideally, $x_0 = A_x = V_0/2$, but for several reasons, such as unequal beam powers and unequal wave-front curvatures in the returning beams from the reference and the measurement arm, the visibility is $A_x/x_0 < 1$. The sensitivity of MI

$$S = \frac{dx}{du} = \frac{4\pi A_x}{\lambda}\cos p \quad (3)$$

changes with the optical phase p, which is an undesired property of the MI. Its largest value $S_{\max} = 4\pi A_x/\lambda$ corresponds to the steepest slope in the interference curve, which occurs midway between the maximum and the minimum of the detected signal. With a typical AC amplitude of about 1 V, the highest sensitivity is 20 mV/nm.

A displacement of $\pm\lambda/16$ from the point of best sensitivity (see the gray-shaded region in Fig. 2) already degrades the sensitivity by about 30%, whereas at $\pm\lambda/8$ from the point of best sensitivity, the signal of the MI reaches the fully constructive/destructive interference (the peaks and troughs in Fig. 2b). Here, the MI is insensitive to nanometric displacements.

The optical phase is given by

$$p(t) = \arcsin\frac{x(t) - x_0}{A_x}. \quad (4)$$

It appears that the AC amplitude $A_x = (x_{\max} - x_{\min})/2$ and the DC offset $x_0 = (x_{\max} + x_{\min})/2$ have to be determined before the measurements are made if the displacement is not long enough that the extrema $x_{\max}$ and $x_{\min}$ of the interference are reached. In this case, a synthetic displacement surpassing one fringe must be accomplished prior to the measurements to acquire the normalization parameters A_x and x_0.

A MI is used either to count interference quanta—fringes—or to measure subtle subfringe displacements in

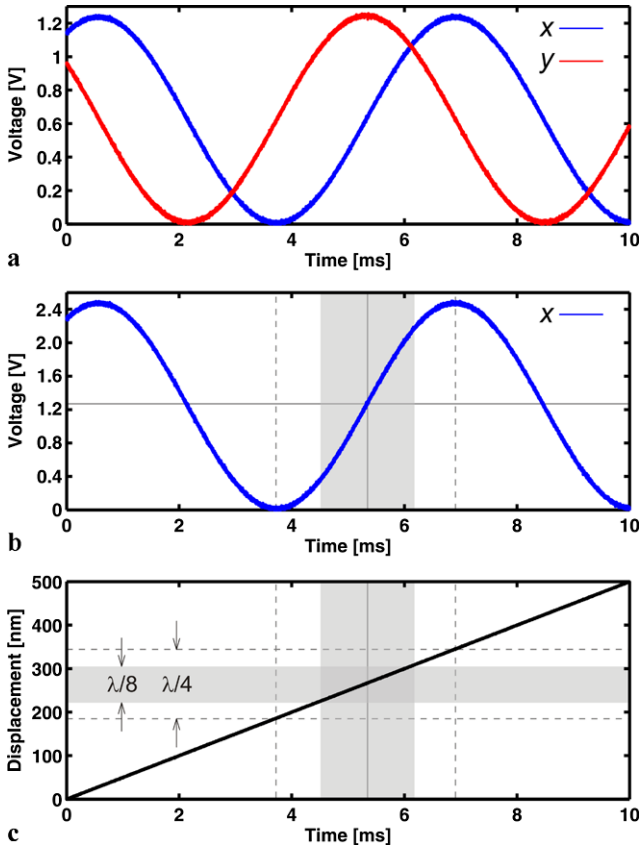

Fig. 2 The measurement of the 500-nm-long uniform displacement of a mirror mounted on a piezoelectric transducer using HQLI. (**a**) HQLI quadrature signals x and y. (**b**) A single signal of MI. It can only be used to monitor a displacement shorter than $\lambda/8$ if it is locked midway between the maximum and minimum of the interference fringe, as is depicted with the *gray-shaded region*. (**c**) The linear displacement obtained from the HQLI quadrature signals x and y

the nearly linear range $\pm\lambda/16$ from the point of the highest sensitivity. In the first case, the resolution is poor, namely $\lambda/2$, while in the second case, the total displacement is limited to $<\lambda/8$.

The limiting resolution of the detected displacement due to quantum laser amplitude noise (photon shot noise), which is dominant over the detector noise if the laser power is about 1 mW, is given by [3, 11]

$$u_{\min} = \frac{\lambda}{4\pi} p_{\min} = \frac{\lambda}{4\pi}\sqrt{\frac{2hc\Delta f}{\lambda\eta P_L}}, \tag{5}$$

where h is Planck's constant, c is the speed of light in a vacuum, Δf is the measurement bandwidth, η is the detector quantum efficiency, and P_L is the output power of the laser beam of wavelength λ. The smallest detectable displacement $u_{\min}$ using a He-Ne red light of $\lambda = 632.8$ nm, and a typical quantum efficiency of about $\eta = 0.8$, can be calculated using the following equation:

$$u_{\min} = 4.5 \times 10^{-5}\sqrt{\frac{\Delta f}{P_L}}\ \mathrm{pm\,J^{1/2}}. \tag{6}$$

Given that the total displacement of MI is $\lambda/8$, the dynamic range is

$$\mathrm{DNR} = \frac{\pi}{2}\sqrt{\frac{\lambda\eta P_L}{2hc\Delta f}}. \tag{7}$$

Again, this can be reduced to

$$\mathrm{DNR} = 1.8 \times 10^{9}\sqrt{\frac{P_L}{\Delta f}}\ \mathrm{J^{-1/2}}, \tag{8}$$

for $\lambda = 632.8$ nm and $\eta = 0.8$.

In applications such as the measurement of laser-induced mechanical waves on samples with low reflectivity, the bandwidth can be as high as 200 MHz and the maximum laser power reaching the photodiodes about 10 μW, yielding the minimum resolvable displacement of 0.2 nm and a dynamic range of only 4×10^2.

Due to long-term mechanical vibrations and drift, the starting point of a MI may be anywhere on its interference curve. If high-frequency nanometric displacements, such as laser ultrasound [2, 12–14], are to be measured with the MI, the interferometer has to be locked to the point of the highest sensitivity by a feedback loop that compensates for low-frequency ambient displacements. There are many ways to realize this compensation [13]. In our ACMI, we made use of the low-frequency part (<1 kHz) of the signal and fed it to the proportional integral-derivative (PID) controller. The controller's output is used to drive the PZT that holds the mirror in the reference arm. A schematic of such a PID-controlled arm-compensated MI (ACMI) is shown in Fig. 1a. A detailed description of the ACMI can be found elsewhere [6]. It should be noted that the low-frequency components of the measured displacement are not visible in the detected signal, but can, nevertheless, be reproduced by monitoring the feedback signal delivered to the PZT.

The main idea in overcoming the drawback of the MI is to have two signals that are phase-shifted by 90°. In practice, this means that if one signal is insensitive to displacement, the other is at the point of the highest sensitivity and vice versa. We will show that switching between two such signals in phase quadrature does not have to be discrete. It can be done in a smooth fashion that preserves the overall sensitivity of the HQLI, shown in Fig. 1b. The detailed operation of an ideal HQLI is theoretically described in [4]. In short, two phase-shifted signals are obtained by separating two perpendicular polarizations with a polarizing beamsplitter, where an additional optical path length of a quarter

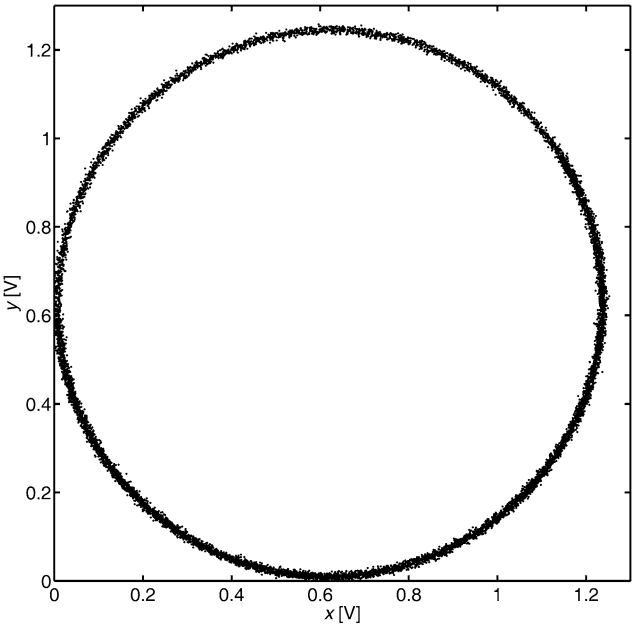

Fig. 3 The Lissajous circle corresponding to the optimally aligned HQLI's photodiode signals in Fig. 2a. The signals possess DC offsets, have matching AC amplitudes and are in exact quadrature

wavelength in one polarization is achieved by a double-pass through a properly rotated octadic-wave plate placed in the reference arm. Effectively, this yields two ideal signals of the form

$$x = \frac{V_0}{4}(1 + \sin p), \tag{9a}$$

$$y = \frac{V_0}{4}(1 + \cos p). \tag{9b}$$

Figure 2 shows the displacement measurement of a mirror mounted on a linearly driven PZT. A pair of voltage signals in quadrature obtained with the HQLI is shown in Fig. 2a, while Fig. 2b shows a single photodiode response for the MI. Apart from its higher amplitude, this MI signal is similar to the x-signal of the HQLI. In contrast to the MI, which loses linearity and sensitivity when the measured displacement exceeds $\lambda/8$ (the gray-shaded area in Figs. 2b and 2c), the HQLI has a constant sensitivity. The displacement in Fig. 2c was obtained with the HQLI. When the HQLI's signals have equal AC amplitudes and are in perfect quadrature, the Lissajous representation of these signals forms a circle, as shown in Fig. 3.

The vector (x, y) draws out a full circle—the Lissajous figure of the signals x and y—if the optical phase p changes by more than 2π (see Fig. 3). Thus, one revolution of the rotating vector path corresponds to a phase change of 2π. This is equivalent to a displacement by $\lambda/2$ of the measuring surface or one fringe, so the measurement of the displacement becomes possible by following the phase of the rotating vector. As the measuring surface moves forward (toward the NBS), the vector rotates in the counterclockwise direction. If it moves backward (away from the NBS), the vector rotates in the clockwise direction. The direction of motion is therefore easily discernable because in one direction the signal x leads the signal y, while in the opposite direction the role of the signals is interchanged.

In contrast to the MI, the sensitivity of the HQLI with ideal signals is constant

$$S = \sqrt{\left(\frac{dx}{du}\right)^2 + \left(\frac{dy}{du}\right)^2} = \frac{4\pi A}{\lambda}\sqrt{\cos^2 p + \sin^2 p} = \frac{4\pi A}{\lambda} \tag{10}$$

and equal to one half of the highest sensitivity of the MI [15].

3 HQLI in high-amplitude laser ultrasonics

We will first explain how our practical realization of the HQLI efficiently solves the scale nonlinearity and later demonstrate its performance on the measurement of high-frequency and high-amplitude laser-induced ultrasound.

Although the HQLI is optimally aligned, in a practical realization the signals are still slightly distorted. Their general form is written as

$$x = x_0 + A_x \sin(p + p_0), \tag{11a}$$

$$y = y_0 + A_y \cos p. \tag{11b}$$

The parameters $\{x_0, y_0, A_x, A_y, p_0\}$, known as the common nonlinearities, are: the DC offsets (x_0, y_0), the AC amplitudes (A_x, A_y) and the lack of quadrature p_0. They are found in every HQLI and must be effectively determined and corrected by an online/offline signal processing [16–21] to achieve a better accuracy.

When the common nonlinearities are taken into account, the ideal Lissajous circle shown in Fig. 3 is deformed into an ellipse (see Figs. 4 and 5). The sensitivity is no longer constant, but exhibits a fringe-periodic deviation from the constant value. The circle is distorted into an ellipse if the AC amplitudes are not equal and/or the signals lack the quadrature.

Figure 4 shows the displacement measurement of a mirror mounted on a linearly driven PZT. In this case, the HQLI was intentionally misaligned, so that its signals have *unequal AC amplitudes*, but are in perfect quadrature. The ratio between the AC amplitudes, shown in Fig. 4a, is $A_x/A_y = 1.72$. The measured displacement for this case is shown in Fig. 4b with the green curve. The black curve in Fig. 4b shows the reference displacement, measured with a perfectly aligned interferometer. The comparison between the

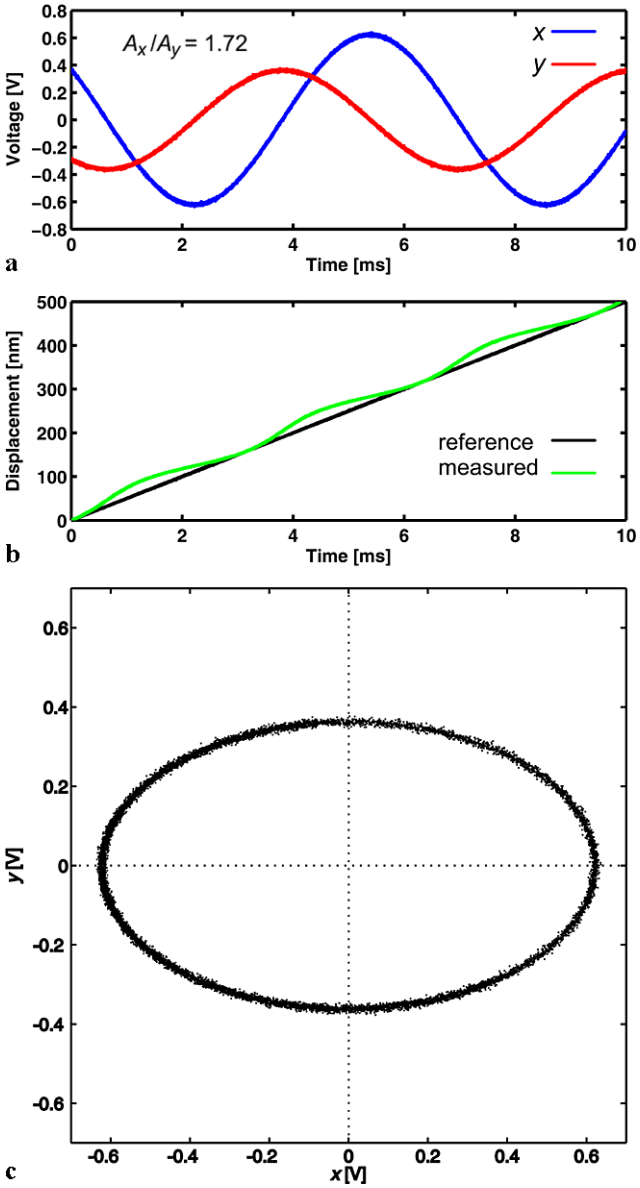

Fig. 4 The measurement of the 500-nm-long uniform displacement with intentionally misaligned HQLI. (**a**) The HQLI photodiode signals with subtracted DC offsets are in quadrature but have unequal AC amplitudes ($A_x/A_y = 1.72$). (**b**) The measured displacement (the *green line*) and the reference displacement (the *black line*) that is obtained by the perfectly aligned HQLI. (**c**) The Lissajous ellipse showing the flattening of an ideal circle due to the *unequal AC amplitudes*

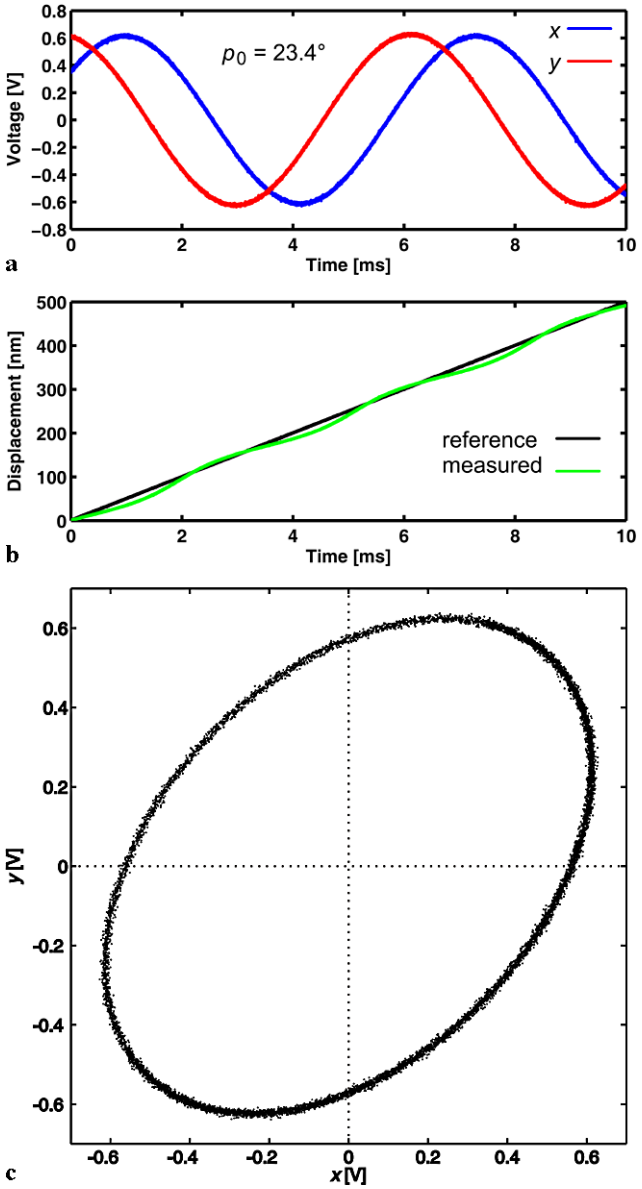

Fig. 5 The measurement of the 500-nm-long uniform displacement with intentionally misaligned HQLI. (**a**) The HQLI photodiode signals with subtracted DC offsets lack the quadrature ($p_0 = 23.4°$) but have equal AC amplitudes. (**b**) The measured displacement (the *green line*) and the reference displacement (the *black line*) that is obtained by the perfectly aligned HQLI. (**c**) The Lissajous ellipse showing the distortion of an ideal circle due to the *lack of quadrature*

measured and the reference displacement clearly shows a two-cycle-per-fringe periodic displacement-error. The corresponding Lissajous curve of the HQLI with *unequal AC amplitudes* is shown in Fig. 4c. In this case, the axes of the ellipse have different lengths, but remain aligned with the x- and y-axis.

To show the displacement error due to the imperfect quadrature, we measured a linear displacement using the HQLI whose signals have equal AC amplitudes, while they *lack the quadrature* ($p_0 = 23.4°$). The corresponding measured displacement obtained with the intentionally misaligned HQLI is shown with the green curve in Fig. 5b. Again, the black curve in Fig. 5b shows the reference displacement, measured with a perfectly aligned interferometer. In the case of the *lack of quadrature,* the Lissajous curve distorts the circle into the ellipse, shown in Fig. 5c. When the AC amplitudes are equal but the signals are not in quadrature, the corresponding Lissajous curve is an ellipse with unequal axes-lengths whose orientations are $\pm 45°$ with respect to the abscise.

The illustrated nonlinearities are intentionally exaggerated so that their effect on the displacement error is easily distinguishable in Figs. 4 and 5. In practical arrangements, it is desirable that the nonlinearities are removed by a proper alignment of optical components [15, 22]. However, residual common nonlinearities are still present. Although they are significantly smaller, they still have to be corrected by an appropriate signal processing to maximize the resolution.

In the ideal case, the optical phase is obtained by the basic unwrapping equation [23]:

$$p = \arctan\frac{x}{y} + m\pi \quad \text{and} \quad m = 0, \pm 1, \pm 2, \ldots. \tag{12}$$

Inserting the signals that include the common nonlinearities (11) into (12) gives rise to a second-order, two-cycle-per-fringe periodic error in the calculated displacement. To correct this periodic error, we need to obtain the parameters $\{x_0, y_0, A_x, A_y, p_0\}$ from the measured signals and then insert them into the modified unwrapping equation

$$p = \arctan\left(\cos^{-1} p_0 \frac{A_y}{A_x}\frac{x - x_0}{y - y_0} - \tan p_0\right) + m\pi. \tag{13}$$

According to Heydemann [9], the most convenient way to obtain the set of nonlinearities $\{x_0, y_0, A_x, A_y, p_0\}$ is to transform the signals from their parametric form (10) into an implicit form

$$ax^2 + 2bxy + cy^2 + 2dx + 2fy + g = 0 \tag{14}$$

with the conic coefficients $\{a, b, c, d, f, g\}$ by removing the phase p from the parametric equations. The reason behind this transformation lies in the fact that fitting elliptically scattered data to obtain the parameters $\{x_0, y_0, A_x, A_y, p_0\}$ is computationally less expensive when they are represented in the general conic (14). A good balance between the accuracy of the fit and the computational efficiency is given by the least-squares fitting method, which is based on minimizing the algebraic distance. Our data processing employs the ellipse-specific least-squares fitting (ESF) developed by Harker et al. [10]. In comparison to the traditional least-squares fitting methods [7, 9, 16, 17, 19–21], such a processing of the HQLI signals provides nanometric accuracy of the interferometer, provided the data draws merely a quarter-arc of an ellipse. In addition, due to the special quadratic constraint imposed on the conic coefficients, this method never returns nonellipse conics, such as a hyperbola. This makes the fitting more robust. This method is also very stable, because the data is first normalized (scaled and mean-free). Moreover, the matrix computation effort is reduced by matrix partitioning, which speeds up the fitting.

The above described signal processing and the fast, 200-MHz photodiodes enable measurements of laser-induced high-amplitude and high-frequency mechanical motion. To demonstrate this and to confirm that the developed HQLI efficiently overcomes the limitations of the ACMI, we present an example of the epicentral detection of laser ultrasound in an Al plate.

The experimental setup is shown in Fig. 1. The high-amplitude ultrasound was induced by a Q-switched Nd:YAG laser operating at 1064 nm, capable of producing 10-ns-long pulses with a maximum energy of 300 mJ. The excitation laser pulse was focused to a 1-mm-diameter spot on the front surface of an 8-mm-thick aluminum plate. The intensity of the pulse on the front surface of the aluminum sample was high enough to surpass the ablation threshold, thus producing strong, longitudinal, ultrasonic wave propagating predominantly in the normal direction. To enhance the linear momentum transfer, the interaction site was covered with water. The direct laser-induced ultrasound, as well as its reflections from the front and the rear surfaces of the plate, was measured with two interferometric methods: the ACMI and the HQLI. The beams of the interferometric and the excitation laser were aligned, thus forming the epicentral position.

The rear-surface displacement shown in Fig. 6a is obtained from the 200-MHz HQLI signals using the described data processing. After $t_L = 1.265$ µs, i.e., the time-of-flight of the longitudinal wave in an 8-mm-thick Al plate, the rear surface experiences a sudden forward motion due to the first arrival of the compressional ultrasonic wave. This surface motion is detected as the first peak, labeled L1 in Fig. 6a. Due to the epicentral position, the other reflections, L3, L5, and L7, are detected with the time period of $2t_L$.

The shaded region in Fig. 6a is presented in Fig. 6b in greater detail. The raw signal measured by the ACMI and stabilized to 0.38 V is shown in Fig. 6c. The dashed horizontal lines in Fig. 6b separate the graph into $\lambda/4$-displacement bands. Within each band, the slope-sign of the displacement (sign of velocity) is either equal (the solid curve) or opposite (the dot-dashed and the dashed curves) with respect to the slope-sign of the ACMI photodiode voltage signal shown in Fig. 6c. Here, the corresponding half-fringe ($\lambda/4$) lines lie at $V_{\min} = 0.13$ V and $V_{\max} = 0.93$ V.

The first arrival of the longitudinal wave (L1) is detected as a 330-nm sharp peak at t_L. As seen in Fig. 6c, its amplitude cannot be determined using a single photodetector as in ACMI, because such an interferometer is insensitive to displacements near $V_{\max}$ and $V_{\min}$. Therefore, we cannot distinguish whether the first arrival is indeed a single peak or whether it is composed of multiple peaks, since the direction of the displacement is indiscernible near the maximum and minimum of the detected signal. The photodiode voltage changes slope-sign in two cases: at the peaks and troughs of the interference or when the measured surface changes the sign of the velocity.

At the first arrival of the compressional high-amplitude ultrasonic wave, the measured surface experiences a sudden forward motion and reaches a velocity that exceeds the

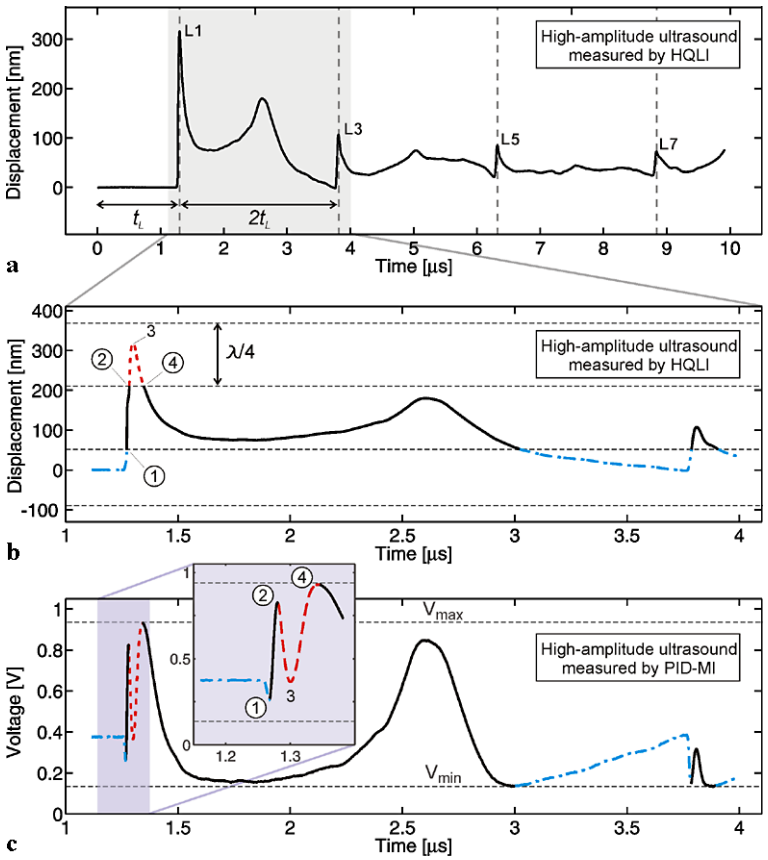

Fig. 6 Comparison between the ACMI and the HQLI during the measurement of the high-amplitude and high-frequency laser-induced ultrasound. (**a**) The displacement of the rear surface of an 8-mm-thick Al plate measured with the HQLI. (**b**) The magnification of the shaded region in (**a**). (**c**) The photodiode signal obtained with the ACMI that corresponds to the measured displacement in (**b**)

frequency range of the photodiodes. When light modulation with frequencies higher than 200 MHz is detected, the amplitudes $A_{x,y}$ of the photodiode signals are reduced. This effect is clearly visible in the inset in Fig. 6c. The encircled numbers indicate the positions where the displacement crosses the $\lambda/4$-displacement bands. Here, the HQLI correctly detects that the velocity does not change sign, even when its raw signals do not touch the lines at $V_{\max}$ and $V_{\min}$ due to high frequencies (the encircled numbers 1 and 2). The velocity of the backward motion is sufficiently reduced so that the photodiode signal crossing the $\lambda/4$-displacement-band (encircled number 4) touches the voltage maximum as expected when the HQLI operates within the frequency bandwidth. The number 3 indicates the change of sign in the velocity, which is correctly detected by the HQLI.

It is known that the ACMI cannot distinguish the direction of motion once its signal reaches the voltage extrema and it must be used within the frequency bandwidth of the detector. On the other hand, the quadrature detection method used in the HQLI is capable of detecting ultrafast motion exceeding the bandwidth of the photodiodes, provided that both photodiodes have the same gain and frequency-response characteristics. This follows from (13), since in this case the values of x_0, y_0 and p_0 remain unchanged, while the amplitudes A_x and A_y are proportionally reduced, so that the ratio A_y/A_x is also unchanged.

4 Conclusion

In summary, we have presented a single-frequency laser interferometer featuring a wide dynamic range of 10^6, a constant sensitivity, a bandwidth of 200 MHz and a nanometric resolution. This interferometer is based on quadrature detection and uniform fringe subdivision. The quadrature of two orthogonally polarized interference signals in the developed interferometer is achieved by an octadic wave-plate in combination with the linearly polarized laser output and the polarization beamsplitter. To subdivide the fringe linearly, we determined and corrected the periodic deviations, which are common to all homodyne quadrature laser interferometers, with a special data processing based on extracting the parameters describing the nonlinearities with an ellipse-specific, least-squares fitting. This interferometer proved to be a useful tool for measuring high-amplitude ultrasonic waves on moving objects, nanometrology and the calibration of vibration and shock transducers in the subfringe stroke range.

References

1. G.L. Dai, F. Pohlenz, H.U. Danzebrink, K. Hasche, G. Wilkening, Meas. Sci. Technol. **15**, 444 (2004)
2. T. Požar, P. Gregorčič, J. Možina, Opt. Express **17**, 22906 (2009)

3. J. Lawall, E. Kessler, Rev. Sci. Instrum. **71**, 2669 (2000)
4. P. Gregorčič, T. Požar, J. Možina, Opt. Express **17**, 16322 (2009)
5. T. Požar, J. Možina, Stroj. Vestn., J. Mech. Eng. **55**, 575 (2009)
6. T. Požar, J. Možina, Appl. Phys. A, Mater. Sci. Process. **91**, 315 (2008)
7. K.P. Birch, M.J. Downs, Metrologia **30**, 155 (1993)
8. S.J.A.G. Cosijns, PhD Thesis, Technische Universiteit Eindhoven (2004)
9. P.L.M. Heydemann, Appl. Opt. **20**, 3382 (1981)
10. M. Harker, P. O'Leary, P. Zsombor-Murray, Image Vis. Comput. **26**, 372 (2008)
11. A. Neubrand, P. Hess, J. Appl. Phys. **71**, 227 (1992)
12. T. Požar, R. Petkovšek, J. Možina, Appl. Phys. Lett. **92**, 234101 (2008)
13. C.B. Scruby, L.E. Drain, *Laser Ultrasonics* (Hilger, Bristol, 1990)
14. R.J. Dewhurst, Q. Shan, Meas. Sci. Technol. **10**, R139 (1999)
15. T. Požar, P. Gregorčič, J. Možina, Appl. Opt. **50**, 1210 (2011)
16. O. Číp, F. Petrů, Meas. Sci. Technol. **11**, 133 (2000)
17. T. Eom, J. Kim, K. Jeong, Meas. Sci. Technol. **12**, 1734 (2001)
18. T. Keem, S. Gonda, I. Misumi, Q.X. Huang, T. Kurosawa, Appl. Opt. **43**, 2443 (2004)
19. P. Křen, Int. J. Nanotechnol. **4**, 702 (2007)
20. C.M. Wu, C.S. Su, G.S. Peng, Meas. Sci. Technol. **7**, 520 (1996)
21. T. Usuda, M. Dobosz, T. Kurosawa, Nanotechnology **9**, 77 (1998)
22. J. Ahn, J.A. Kim, C.S. Kang, J.W. Kim, S. Kim, Opt. Express **17**, 23299 (2009)
23. T. Usuda, T. Kurosawa, Metrologia **36**, 375 (1999)